Intrinsic optical anisotropy in zinc-blende semiconductor quantum wells

Chun-Nan Chen*
Nano-Photonics Simulation and Computing Laboratory, Department of Electronic Engineering, Far East College, Hsin-Shih Town, Tainan, Taiwan, Republic of China

(Received 24 November 2004; revised manuscript received 22 March 2005; published 1 August 2005)

An analytical $(hk\ell)$-oriented $\mathbf{k}\cdot\mathbf{p}$ method is developed in this paper and applied to calculate the optical transition strength of zinc-blende semiconductor quantum wells. The optical matrix elements and the hole effective masses are presented in analytical forms. Calculations are performed for $In_{0.53}Ga_{0.47}As/InP$ quantum wells oriented in arbitrary growth directions. The in-plane polarization angle is adopted as a key parameter in the calculations performed to explore the variation of the optical transition strength in the well plane. The theoretical results indicate that the largest optical anisotropy of the optical matrix elements in the well plane appears in the (110) surface.

DOI: 10.1103/PhysRevB.72.085305 PACS number(s): 78.55.Cr, 68.65.Fg, 78.67.De

I. INTRODUCTION

Recent advances in growth technologies now enable the growth of high-quality semiconductor heterostructures on substrates with orientations other than the conventional (001) direction.[1–3] Furthermore, the advances made in modern crystal growth technologies for various substrate orientations have motivated a particularly interesting, and that is mainly due to its unique optical and electronic properties. Importantly, one of the unique properties is the optical anisotropy in quantum-confined semiconductor systems. It has been predicted theoretically[1,3–7] that semiconductor heterostructures grown on a substrate with a low symmetry orientation will exhibit anisotropic characteristics. Furthermore, in-plane anisotropy has been confirmed experimentally for epitaxial layers grown on substrates of various orientations, including (110),[8,9] (113),[3,10] and (112)[11] substrates.

General $(hk\ell)$-oriented planes provide a further crucial degree of freedom which gives device designers a greater flexibility when tailoring the band structure of the semiconductor heterostructures used in advanced optical devices.[12–15] However, low-symmetry planes will result in the anisotropy of the optical matrix elements on the growth surface.[1,3,4,6] These non-(001)-oriented planes yield an alteration of the crystal symmetry in the different growth directions and cause a modification of the valence band structure. Many of the optoelectronic devices used in modern optical telecommunication systems require a polarization-independent operation. However, laser diodes are designed in such a way that operation in the polarization direction reduces the threshold current.[14] Therefore, detailed studies of the in-plane optical anisotropy phenomenon are required.

In the theoretical derivation of semiconductors and their heterostructures, the $\mathbf{k}\cdot\mathbf{p}$ approach[16,17] tends to be the most widely adopted since its calculations and application are relatively straightforward. As an alternative to the conventional $\mathbf{k}\cdot\mathbf{p}$ method, an analytic expression for the $\mathbf{k}\cdot\mathbf{p}$ Hamiltonian[7,18,19] can be obtained by expanding the Hamiltonian of the bond orbital model[18–20] (BOM) in a Taylor series with respect to the wave vector $\mathbf{k}$ and then truncating the series to the second order in $\mathbf{k}$. This analytical $\mathbf{k}\cdot\mathbf{p}$ method indicates more physical meanings in the lattice symmetry and easier manipulations in the mathematical calculations used to investigate the optical anisotropy in any $(hk\ell)$ - oriented quantum well (QW) than the conventional $\mathbf{k}\cdot\mathbf{p}$ method.[4,6,15,21] With various refinements, the analytical $\mathbf{k}\cdot\mathbf{p}$ method can provide sophisticated results and can be used to study many problems, including the effects of optical and magnetic fields, and the piezoelectric effects of external stress and internal strain, etc. Therefore, the analytical $\mathbf{k}\cdot\mathbf{p}$ method is expected to be widely adopted due to its conceptual simplicity, operational efficiency, and applied versatility. Importantly, the analytical $\mathbf{k}\cdot\mathbf{p}$ method provides practical formula, which can also be used by experimentalists.

The calculations in the current study are performed analytically with the $\mathbf{k}\cdot\mathbf{p}$ approach, taking the inherent lattice symmetry of the bulk material into account. Explicit mathematical expressions for the optical transition strength of zinc-blende semiconductor QWs are presented. Specifically, one of the goals of the present study is to derive a general quantitative description of the optical transition strength relative to the $(hk\ell)$-, and particularly the (11ℓ)-, substrate surfaces. This study also calculates the effective masses of the hole as a function of the substrate orientation. The effects of arbitrary substrate orientations on the optical properties of zinc-blende semiconductor QWs are explored in detail.

II. THEORETICAL METHOD

In an analytical formalism, the $\mathbf{k}\cdot\mathbf{p}$ matrix elements can be written as[7,18,19]

$$H_{\mathbf{k}\cdot\mathbf{p}}(\mathbf{k})_{\alpha',\alpha}=\sum_j\left\{1-\tfrac{1}{2}(\mathbf{k}\cdot\mathbf{R}_j)^2+i\mathbf{k}\cdot\mathbf{R}_j\right\}\in_{\alpha',\alpha}(j), \quad (1)$$

where $\alpha(=s,x,y,z)$ denotes s-like or p-like basis functions, $\mathbf{k}$ is a wave vector, $\mathbf{R}_j$ with $j=0$–12 is the position vector of the on-site lattice $(j=0)$ or one of the 12 nearest-neighbor lattices $(j=1$–$12)$, and $\in_{\alpha',\alpha}(j)$ is an interaction parameter between bond orbitals of symmetry type α' (located at the relative origin $\mathbf{R}'$) and α (located at one of the lattice sites $\mathbf{R}=\mathbf{R}_j+\mathbf{R}'$ with $(j=1$–$12)$. A total of seven interaction pa-

TABLE I. The interaction parameters (in units of electron-volts).

	E_s	E_p	E_{ss}	E_{sx}	E_{xx}	E_{xy}	E_{zz}
InP	9.260	−4.157	−0.682	0.317	0.484	0.701	−0.016
GaAs	12.990	−4.785	−0.956	0.344	0.565	0.821	0.065
InAs	14.851	−4.646	−1.203	0.360	0.554	0.822	0.054

rameters, $\in_{\alpha',\alpha}$, exist, namely, E_s, E_p, E_{ss}, E_{sx}, E_{xx}, E_{xy}, and E_{zz}, which are listed in Table I.[7,18,19]

The present study applies a conceptually straightforward approach to derive an analytical expression for the momentum matrix elements, $\mathbf{M}_{\mathbf{k}\cdot\mathbf{p}}(\mathbf{k})_{\alpha',\alpha}$. The first-order derivative of the $\mathbf{k}\cdot\mathbf{p}$ Hamiltonian with respect to the wave vector $\mathbf{k}$ is given by[7,22]

$$\boldsymbol{\varepsilon}_\xi \cdot \mathbf{M}_{\mathbf{k}\cdot\mathbf{p}}(\mathbf{k})_{\alpha',\alpha} = \boldsymbol{\varepsilon}_\xi \cdot [\partial H_{\mathbf{k}\cdot\mathbf{p}}(\mathbf{k})_{\alpha',\alpha}/\partial \mathbf{k}] = \sum_j \{-[\mathbf{k}\cdot\mathbf{R}_j]R_{j,\xi} + iR_{j,\xi}\} \in_{\alpha',\alpha}(j), \quad (2)$$

where $\boldsymbol{\varepsilon}_\xi$ is the unit vector of the $\boldsymbol{\xi}$-polarization optical field, $\boldsymbol{\xi}$ (=x, y, or z) is the polarization direction of the optical field, and $R_{j,\xi}$ is the $\boldsymbol{\xi}$-component of the jth position vector, $\mathbf{R}_j$.

The linear combinations of the $H_{\mathbf{k}\cdot\mathbf{p}}(\mathbf{k})_{\alpha',\alpha}$ $[\mathbf{M}_{\mathbf{k}\cdot\mathbf{p}}(\mathbf{k})_{\alpha',\alpha}]$ and the spin-orbit coupling coefficients yield the $H_{\mathbf{k}\cdot\mathbf{p}}(\mathbf{k})_{\nu',\nu}$ $[\mathbf{M}_{\mathbf{k}\cdot\mathbf{p}}(\mathbf{k})_{\nu',\nu}]$ with $|\nu,\mathbf{k}\rangle$ basis functions, where $\nu = |S\rangle\chi_{\sigma=\pm1/2}$, $|3/2,\pm3/2\rangle$, and $|3/2,\pm1/2\rangle$. The $\mathbf{k}\cdot\mathbf{p}$ Hamiltonian, $H_{\mathbf{k}\cdot\mathbf{p}}(\mathbf{k})_{\nu',\nu}$, is presented in Appendix A.

The expansion for the QW state $|n,\mathbf{k}_\parallel\rangle$ is written as

$$|n,\mathbf{k}_\parallel\rangle = \sum_{\nu,k_z} \mathrm{F}_\nu(n,\mathbf{k}_\parallel,k_z)|\nu,\mathbf{k}\rangle, \quad (3)$$

where n is a label for the subband index of the QW, $\mathbf{k}=\mathbf{k}_\parallel + k_z\hat{z}$, and $\mathrm{F}_\nu(n,\mathbf{k}_\parallel,z)$ is the so-called envelope function of the QW state and is given by the following Fourier transform:

$$F_\nu(n,\mathbf{k}_\parallel,z) \equiv \sum_{k_z} F_\nu(n,\mathbf{k}_\parallel,k_z)e^{i\mathbf{k}\cdot\mathbf{R}}. \quad (4)$$

The momentum matrix element between subband states $|n',\mathbf{k}_\parallel\rangle$ and $|n,\mathbf{k}_\parallel\rangle$ is given by[23]

$$\begin{aligned}\boldsymbol{\varepsilon}_\xi \cdot \mathbf{M}_{n',n}(\mathbf{k}_\parallel) &= \sum_{\nu',\nu,\mathbf{k}_z} \mathbf{F}_{\nu'}(n',\mathbf{k}_\parallel,k_z)^*[\boldsymbol{\varepsilon}_\xi \cdot \mathbf{M}_{\mathbf{k}\cdot\mathbf{p}}(\mathbf{k})_{\nu',\nu}]F_\nu(n,\mathbf{k}_\parallel,k_z),\\ &= \boldsymbol{\varepsilon}_\xi \cdot \sum_{\nu',\nu} \left\{ \int dz\, F_{\nu'}(n',\mathbf{k}_\parallel,z)^* \mathbf{O}_{\nu',\nu}(\mathbf{k}_\parallel,z)F_\nu(n,\mathbf{k}_\parallel,z) \right.\\ &\quad \left. + \int dz\, F_{\nu'}(n',\mathbf{k}_\parallel,z)^* \mathbf{Q}_{\nu',\nu}(\mathbf{k}_\parallel,z)\left[-i\frac{d}{dz}F_\nu(n,\mathbf{k}_\parallel,z)\right]\right\},\end{aligned} \quad (5)$$

where the superscript * denotes the Hermitian conjugate, the explicit expressions of the matrix elements $\mathbf{O}_{\nu',\nu}(\mathbf{k}_\parallel,z)$ and $\mathbf{Q}_{\nu',\nu}(\mathbf{k}_\parallel,z)$ are given in Appendix B.

The Hamiltonian for arbitrary crystallographic orientations is obtained by rotating the (001) Hamiltonian from the (x,y,z) lattice coordinate system to the (x',y',z') coordinate system. Here, the z' axis is the direction normal to the growth surface, $(hk\ell)$. An appropriate transformation matrix for this rotation is written as[24]

$$\mathbf{U} = \begin{bmatrix} \cos\alpha\cos\beta\cos\gamma - \sin\alpha\sin\gamma & -\sin\alpha\cos\beta\cos\gamma - \cos\alpha\sin\gamma & \sin\beta\cos\gamma \\ \cos\alpha\cos\beta\sin\gamma + \sin\alpha\cos\gamma & -\sin\alpha\cos\beta\sin\gamma + \cos\alpha\cos\gamma & \sin\beta\sin\gamma \\ -\cos\alpha\sin\beta & \sin\alpha\sin\beta & \cos\beta \end{bmatrix} \quad (6)$$

where the angles β (=$\tan^{-1}\sqrt{h^2+k^2}/\ell$) and γ (=$\tan^{-1}k/h$) represent the polar and azimuthal angles, respectively, of the z' direction relative to the (x,y,z) lattice coordinate system. The rotation is specified by its angles α,β,γ. The growth direction, z', is determined by the rotation of the β and γ angles, while the in-plane direction is governed by the rotation of the α angle.

Let $(k_{x'},k_{y'},k_{z'})$ and (k_x,k_y,k_z) be the components of a vector $\mathbf{k}$ in the (x',y',z') and (x,y,z) coordinate systems, respectively. The relationship between these components is given by a rotational matrix, $\mathbf{U}$, i.e.,

$$\begin{bmatrix} k_{x'} \\ k_{y'} \\ k_{z'} \end{bmatrix} = \begin{bmatrix} U_{11} & U_{21} & U_{31} \\ U_{12} & U_{22} & U_{32} \\ U_{13} & U_{23} & U_{33} \end{bmatrix} \begin{bmatrix} k_x \\ k_y \\ k_z \end{bmatrix}, \quad (7)$$

where U_{ij} with i,j=1–3 are elements of the rotational matrix, $\mathbf{U}$. From Eq. (7), the x', y', and z' directions are explicitly represented as expressions in the crystallographic coordinate system.

III. RESULTS AND DISCUSSION

A. Intrinsic optical anisotropy of zinc-blende semiconductors

The momentum matrix element, $\mathbf{M}$, is expressed in terms of an expected value of a momentum operator, $\hat{\mathbf{p}} = (\mathrm{P}_x, \mathrm{P}_y, \mathrm{P}_z)$. The component of $\mathbf{M}$ parallel to the light's electrical field contributes to the light waves as a gain or loss by the square of the scalar product $|\boldsymbol{\varepsilon}\cdot\mathbf{M}|^2$, where $\boldsymbol{\varepsilon}$ is a vector denoting the direction of the light polarization. The squared momentum matrix elements of zinc-blende semiconductors can be written as[25]

$$|\boldsymbol{\varepsilon}\cdot\mathbf{M}|^2_{c\text{-}hh} = \tfrac{1}{2}(1-\cos^2\beta)\mathrm{P}^2_{cv} \tag{8a}$$

for the *c-hh* interband transition, and as

$$|\boldsymbol{\varepsilon}\cdot\mathbf{M}|^2_{c\text{-}lh} = \left(\tfrac{1}{6}+\tfrac{1}{2}\cos^2\beta\right)\mathrm{P}^2_{cv} \tag{8b}$$

for the *c-lh* interband transition, where *c*, *hh*, and *lh* denote the conduction, heavy-hole, and light-hole bands, respectively, β is the angle between the electron wave vector, $\mathbf{k}$, and the light-polarization vector, $\boldsymbol{\varepsilon}$, and P_{cv} is a momentum matrix parameter between the orbital "*s*" and "*p*" states. Owing to the symmetry phenomenon of the *p*-like functions, the interband matrix elements are given as

$$P_{cv} = |\langle S|P_x|X\rangle| = |\langle S|P_y|Y\rangle| = |\langle S|P_z|Z\rangle|, \tag{9}$$

while all the remaining matrix elements are equal to zero.

Figures 1(a) and 1(b) illustrate the *c-hh* and *c-lh* transition strengths for arbitrary polarization light, respectively. The results indicate a strong polarization dependence of the electron-light interaction. It can be seen that the inter-band transition strength is dependent only on the angle β between the vector $\boldsymbol{\varepsilon}$ and the vector $\mathbf{k}$.

Truncating the $\mathbf{k}\cdot\mathbf{p}$ Hamiltonian in a matrix form and retaining only the Γ_8 band gives the 4×4 Luttinger–Kohn Hamiltonian. At $k_{x'}=k_{y'}=0$,[26] the 4×4 $\mathbf{k}\cdot\mathbf{p}$ Hamiltonian for holes in an epilayer (or bulk) grown along the $[hk\ell]$ - direction [in the basis ordering $|3/2,3/2\rangle, |3/2,1/2\rangle, |3/2,-1/2\rangle, |3/2,-3/2\rangle$] is given by

$$\mathbf{H}_{\mathbf{k}\cdot\mathbf{p}}(k_{x'}=k_{y'}=0) = (E_p + 8E_{xx} + 4E_{zz}) - \frac{a^2}{4}k_z^2\left\{\frac{4}{3}(2E_{xx}+E_{zz})\times\begin{bmatrix}1&0&0&0\\0&1&0&0\\0&0&1&0\\0&0&0&1\end{bmatrix} + \left[(E_{xx}-E_{zz}-2E_{xy})\sin^2\beta(2-\Omega) - \frac{2}{3}(E_{xx}-E_{zz})\right]\times\begin{bmatrix}1&0&0&0\\0&-1&0&0\\0&0&-1&0\\0&0&0&1\end{bmatrix} + (E_{xx}-E_{zz}-2E_{xy})\left(\frac{1}{\sqrt{3}}\sin\beta\right)\times\begin{bmatrix}0&\mathrm{S}&\mathrm{T}&0\\\mathrm{S}^*&0&0&\mathrm{T}\\\mathrm{T}^*&0&0&-\mathrm{S}\\0&\mathrm{T}^*&-\mathrm{S}^*&0\end{bmatrix}\right\}, \tag{10}$$

where

$$\Omega = \sin^2\beta(\cos^4\gamma + \sin^4\gamma + 1), \tag{11a}$$

$$\mathrm{S} = (\cos\alpha + i\sin\alpha)\left[2\cos\beta(1-\Omega) - i\sin^2\beta\left(\tfrac{1}{2}\sin 4\gamma\right)\right], \tag{11b}$$

$$\mathrm{T} = -(\cos\alpha + i\sin\alpha)^2\sin\beta\left[2(\cos^4\gamma+\sin^4\gamma) - \Omega + i\cos\beta\left(\tfrac{1}{2}\sin 4\gamma\right)\right], \tag{11c}$$

and "*a*" is the lattice constant.

According to the secular expression given in Eq. (10), the explicit forms of the eigenvalues and eigenvectors, which coincide exactly with analytical results of Merkulov *et al.*,[27] are given by

$$E_\pm = (E_p + 8E_{xx} + 4E_{zz}) - \frac{a^2}{4}k_z^2\left\{\frac{4}{3}(2E_{xx}+E_{zz}) \pm \frac{1}{\sqrt{3}}(E_{xx}-E_{zz}-2E_{xy})\Delta\sin\beta\right\} \tag{12}$$

for the doubly degenerate eigenvalues, and by

$$|\nu_\pm\rangle = \frac{1}{N}\begin{bmatrix}(G\pm\Delta)\\(S^*+T)\\(-S+T^*)\\(G\pm\Delta)\end{bmatrix} \tag{13}$$

for the corresponding eigenvectors, where

$$G = \frac{(E_{xx}-E_{zz}-2E_{xy})\sin^2\beta(2-\Omega) - \frac{2}{3}(E_{xx}-E_{zz})}{(E_{xx}-E_{zz}-2E_{xy})\frac{1}{\sqrt{3}}\sin\beta}, \tag{14a}$$

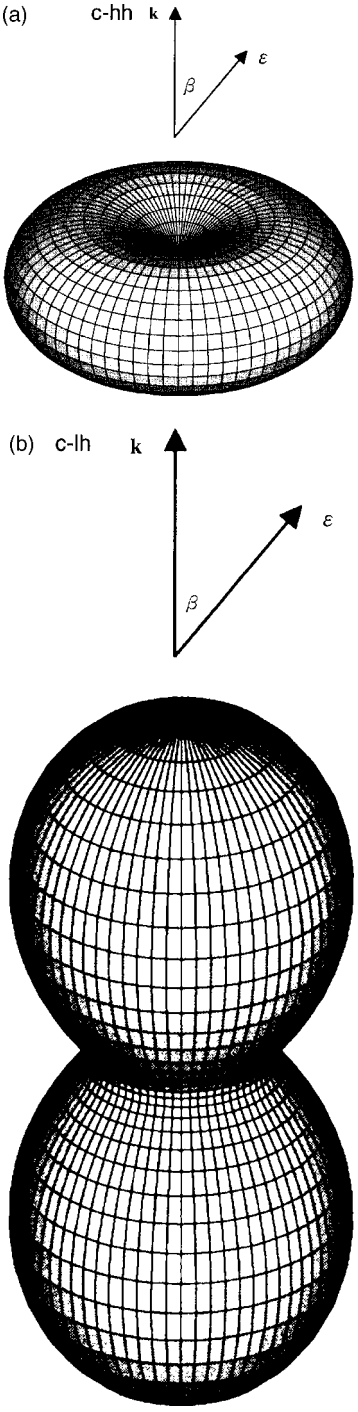

FIG. 1. Optical transition strengths of (a) *c-hh* and (b) *c-lh* transitions as a function of the angle between the electron wave vector and the polarization vector for zinc-blende semiconductor materials.

$$\Delta = \sqrt{G^2 + SS^* + TT^*}, \tag{14b}$$

and

$$N^2 = 2(G \pm \Delta)^2 + |(S^* + T)|^2 + |(-S + T^*)|^2. \tag{14c}$$

Note that throughout this paper, the upper sign (+) refers to *hh*, while the lower sign (−) refers to *lh*.

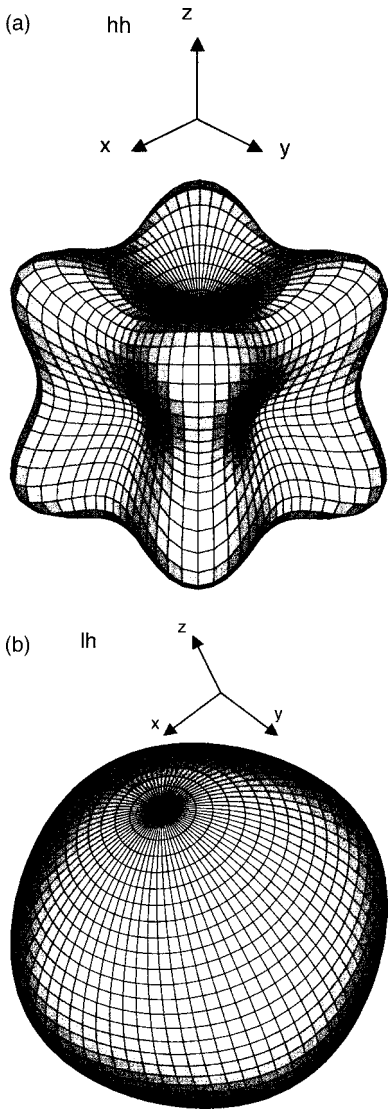

FIG. 2. Longitudinal effective masses in $(hk\ell)$ $In_{0.53}Ga_{0.47}As$ epitaxial layers for (a) *hh* and (b) *lh* transitions as a function of arbitrary growth direction in three-dimensional space.

From Eq. (12), it is possible to derive the following analytical formula for the effective hole-masses $(m'_{\pm})$ along the growth direction $(z'$ axis). Expressed in terms of BOM parameters, $\in_{\alpha',\alpha}$, the effective hole masses $(m'_{\pm})$ for both *hh*(+) and *lh*(−) along the $[hk\ell]$ growth-direction and wave-vector $k_{z'}$ can be written in units of free electron mass, (m), as

$$\frac{1}{m'_{\pm}} = \frac{a^2}{2^2}\left\{\frac{4}{3}(2E_{xx} + E_{zz}) \pm \frac{1}{\sqrt{3}}(E_{xx} - E_{zz} - 2E_{xy})\Delta \sin\beta\right\}. \tag{15}$$

The orientation-dependent effective hole masses along the $[hk\ell]$-growth direction can be examined using Eq. (15). The calculated results of the *hh* and *lh* effective masses as a function of the growth direction are shown in Figs. 2(a) and 2(b), respectively, for $In_{0.53}Ga_{0.47}As$ expitaxial layers. The *hh* effective mass is found to have a strong dependence on the

substrate orientation. However, this is not the case for the *lh* effective mass. It is shown that the *hh* effective mass exhibits a maximum value in samples grown along the [111] direction, and a minimum value in samples grown along the [001] direction.

The $(hk\ell)$-oriented Hamiltonian in the QW structure at the zone center can be obtained by setting $k_{z'}=-i(\partial/\partial z')$ and adding a QW potential profile in Eq. (10). In the next section, this study adopts an infinite-barrier-height approximation, in which $k_{z'}$ can take only discrete values of $n\pi/L$, where n is the subband index and L is the well width.[4,28] Therefore, the analytical $\mathbf{k}\cdot\mathbf{p}$ formalism can be applied to explore the orientation-dependent characteristics of the semiconductor QWs at the zone center. The matrix of this $(hk\ell)$-oriented Hamiltonian becomes diagonal when the azimuthal angle γ is equal to 45° (when $h=k=1$) and the polar angle β is equal to 0° (when $\ell=\infty$) or $\sin^{-1}\sqrt{2}/\sqrt{3}\approx 54.7°$ (when $\ell=1$), corresponding to the two cases where the QWs are oriented to the (001) or (111) surface, respectively. Therefore, the *hh* and *lh* states at the zone center along the [001]-growth and [111]-growth directions are given by the pure eigenstates of the z component of the angular momentum, m_j. For orientations other than (001) and (111), the nonzero off-diagonal matrix elements imply that the *hh* and *lh* states are mixtures of $m_j=\pm 1/2$ and $m_j=\pm 3/2$ components, even at the zone center. The effect of zone-center mixing yields the anisotropy properties such as hole mass and optical transition strength. An analysis shows that this phenomenon can be attributed to a low-symmetry perturbation of the crystal lattice.

B. Momentum matrix elements under infinite-barrier-height approximation

When adopting an infinite-barrier-height and envelope-function approximations, the QW envelope functions for the conduction and valence bands become simple sinusoidal waves. Thus the overlap integral of the envelope functions is always unity for the allowed interband transitions. Consequently, the momentum matrix elements are independent of the envelope functions, which are expressed only as cell-periodic parts in the Bloch functions.[3–5] Furthermore, another approximation used in this section is that the hole eigenatates are independent of the well width of the QWs, and thus the linear-combination coefficients of the hole eigenstates expanded in the $|3/2,\pm 3/2\rangle$ and $|3/2,\pm 1/2\rangle$ basis set are well-width independent. In this approximation, the difference in the $\mathbf{k}\cdot\mathbf{p}$ parameters of the well and the barrier layers is neglected, which is essential for interface mixing between heavy-hole and light-hole eigenstates.[3,5,28] By using the hole eigenstates as the new basis set, the $(hk\ell)$-oriented Hamiltonian at the Γ_8 band in Eq. (10) becomes diagonal. In the presented approximations, the squared momentum matrix elements at the zone center for the x', y', and z' polarizations can be calculated as[3–5,28]

$$|M_{x'}|^2=\frac{1}{N^2}\left|-\frac{1}{\sqrt{2}}(G\pm\Delta)+\frac{1}{\sqrt{6}}(-S+T^*)\right|^2P_{cv}^2+\frac{1}{N^2}\left|\frac{1}{\sqrt{2}}(G\pm\Delta)-\frac{1}{\sqrt{6}}(S^*+T)\right|^2P_{cv}^2, \tag{16a}$$

$$|M_{y'}|^2=\frac{1}{N^2}\left|-\frac{1}{\sqrt{2}}(G\pm\Delta)-\frac{1}{\sqrt{6}}(-S+T^*)\right|^2P_{cv}^2+\frac{1}{N^2}\left|-\frac{1}{\sqrt{2}}(G\pm\Delta)-\frac{1}{\sqrt{6}}(S^*+T)\right|^2P_{cv}^2, \tag{16b}$$

and

$$|M_{z'}|^2=\frac{2}{3N^2}|(-S+T^*)|^2P_{cv}^2+\frac{2}{3N^2}|(S^*+T)|^2P_{cv}^2, \tag{16c}$$

respectively.

Meanwhile, the squared momentum matrix elements can also be expressed as

$$|M_{x'}|^2=\left(\frac{1}{N^2}\right)\left\{\frac{b^2}{3}+\left(\frac{d}{\sqrt{3}}-f\right)^2+\frac{c^2}{3}+\frac{e^2}{3}\right\}\times P_{cv}^2, \tag{17a}$$

$$|M_{y'}|^2=\left(\frac{1}{N^2}\right)\left\{\frac{b^2}{3}+\left(\frac{d}{\sqrt{3}}+f\right)^2+\frac{c^2}{3}+\frac{e^2}{3}\right\}\times P_{cv}^2, \tag{17b}$$

and

$$|M_{z'}|^2=\frac{4}{3}\left(\frac{1}{N^2}\right)(b^2+c^2+d^2+e^2)\times P_{cv}^2, \tag{17c}$$

respectively, where

$$b=2\cos\alpha\cos\beta(1-\Omega)+\tfrac{1}{2}\sin\alpha\sin^2\beta\sin 4\gamma, \tag{18a}$$

$$c=2\sin\alpha\cos\beta(1-\Omega)-\tfrac{1}{2}\cos\alpha\sin^2\beta\sin 4\gamma, \tag{18b}$$

$$d=(\sin^2\alpha-\cos^2\alpha)\sin\beta[2(\cos^4\gamma+\sin^4\gamma)-\Omega]+\cos\alpha\sin\alpha\cos\beta\sin\beta\sin 4\gamma, \tag{18c}$$

$$e=-2\cos\alpha\sin\alpha\sin\beta[2(\cos^4\gamma+\sin^4\gamma)-\Omega]+\tfrac{1}{2}(\sin^2\alpha-\cos^2\alpha)\cos\beta\sin\beta\sin 4\gamma, \tag{18d}$$

$$f=(G\pm\Delta), \tag{18e}$$

and

$$\Delta=\sqrt{G^2+b^2+c^2+d^2+e^2}. \tag{18f}$$

Figures 3 and 4 show the calculated results (in units of P_{cv}^2) of the squared optical matrix elements (by setting $\alpha=0°$) as a function of the substrate orientation for the *c-hh* and *c-lh* transitions, respectively. Due to the symmetry of the eight octants, these figures show only the first octant in three-dimensional space. From the two figures, it is clear that the optical properties of the QWs are sensitive to the crystallographic directions of the epitaxial growth. In these squared matrix elements, it is noted that the following conservation rule exists as:

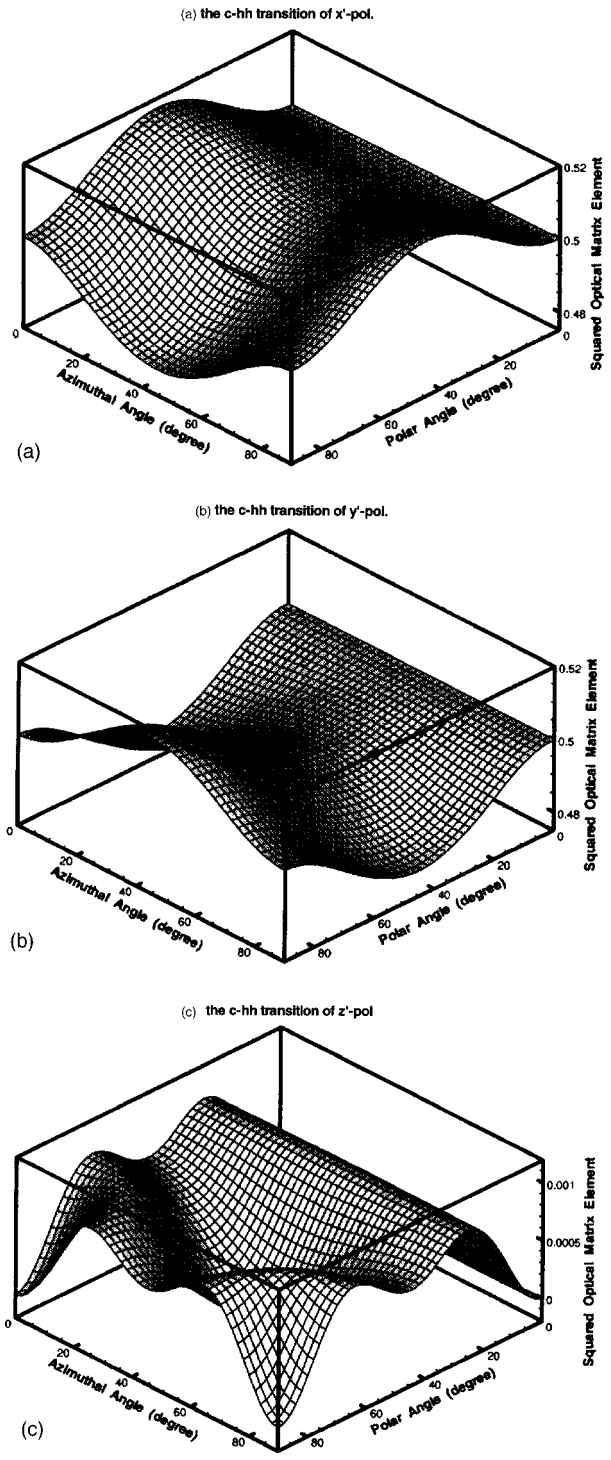

FIG. 3. Squared optical matrix elements (in units of P_{cv}^2) of the *c-lh* transition in $In_{0.53}Ga_{0.47}As$ QWs for (a) x', (b) y', and (c) z'-polarization light.

$$|M_{x'}|_{c\text{-}h}^2 + |M_{y'}|_{c\text{-}h}^2 + |M_{z'}|_{c\text{-}h}^2 = 1P_{cv}^2, \quad (h = hh \text{ or } lh) \tag{19a}$$

and a sum rule exists as

$$|M_{x'}|_{c\text{-}hh}^2 + |M_{x'}|_{c\text{-}lh}^2 = \tfrac{2}{3}P_{cv}^2, \tag{19b}$$

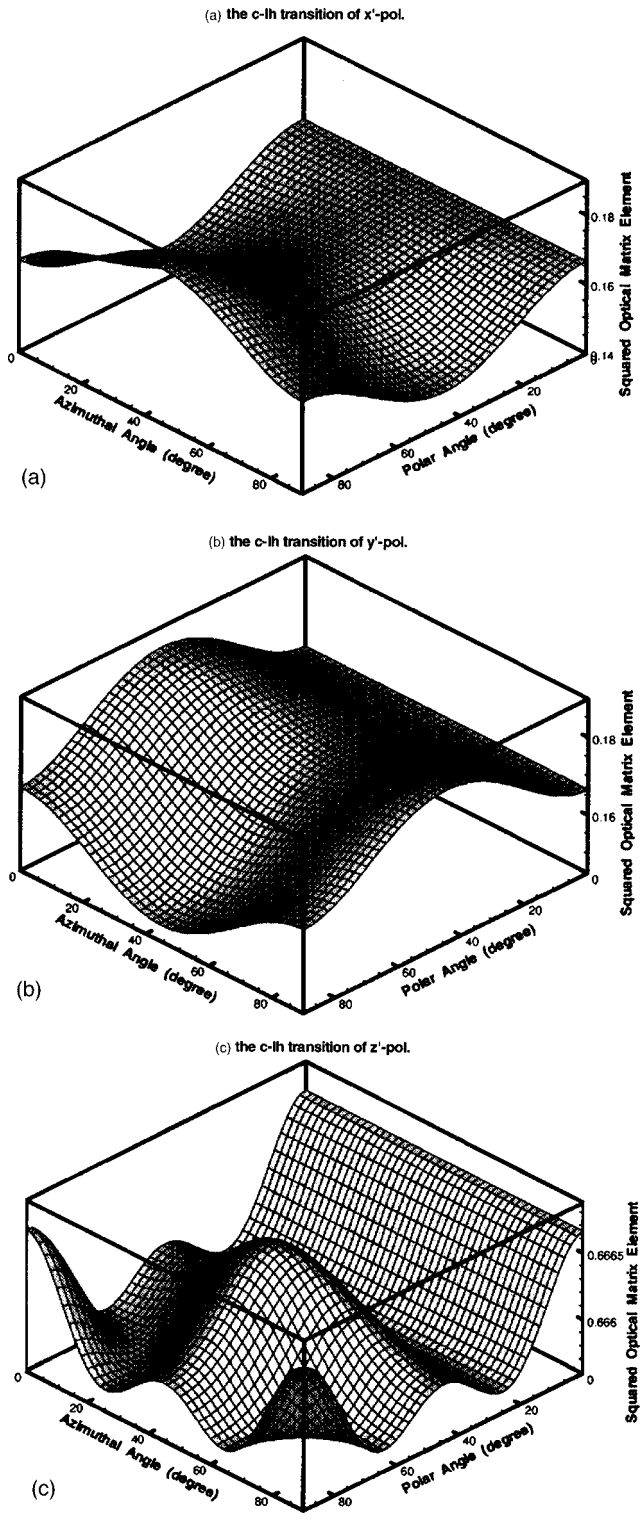

FIG. 4. Squared optical matrix elements (in units of P_{cv}^2) of the *c-hh* transition in $In_{0.53}Ga_{0.47}As$ QWs for (a) x', (b) y', and (c) z'-polarization light.

$$|M_{y'}|_{c\text{-}hh}^2 + |M_{y'}|_{c\text{-}lh}^2 = \tfrac{2}{3}P_{cv}^2, \tag{19c}$$

and

$$|M_{z'}|_{c\text{-}hh}^2 + |M_{z'}|_{c\text{-}lh}^2 = \tfrac{2}{3}P_{cv}^2. \tag{19d}$$

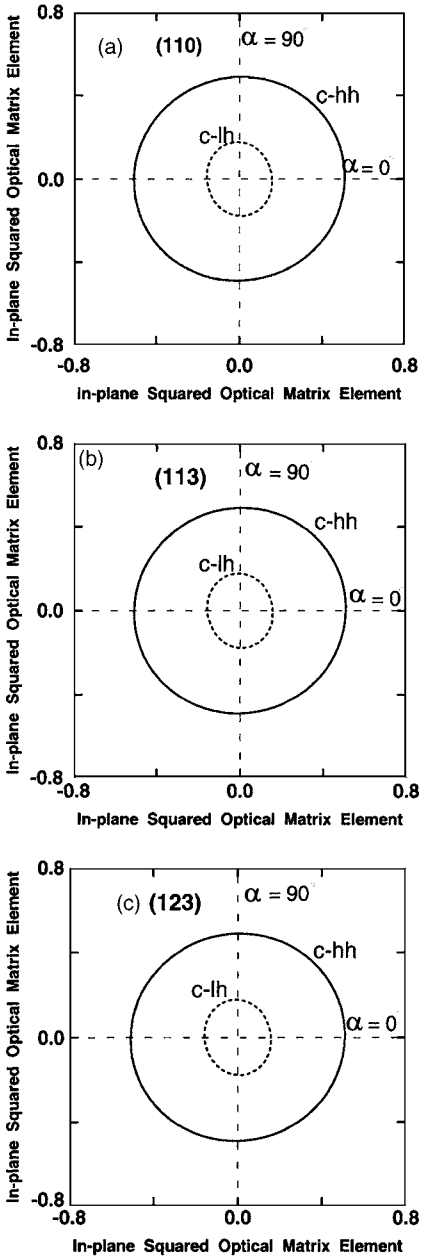

FIG. 5. Squared optical matrix elements (in units of P_{cv}^2) of the in-plane polarization light for both the *c-hh* and *c-lh* transitions in (a) (110), (b) (113), and (c) (123) $In_{0.53}Ga_{0.47}As$ QWs as a function of the in-plane polarization angle.

The conservation and sum rules are in accordance with the predicted results of Eqs. (8a) and (8b). Note that in the calculation of the optical transitions Merkulov *et al.* take into account the mixing of heavy and light holes for the nonzero in-plane wave vector. Notably, this mixing results in nonzero probabilities of some optical transitions (for large values of an in-plane wave vector), which are forbidden in a simplified approximation used in this subsection.[27]

Figures 5(a)–5(c) show the polar plots of the *c-hh* and *c-lh* transition matrix elements on the (110), (113), and (123) well planes, respectively, as a function of the in-plane polarization angle, α. From these figures, it is clear that the in-plane transition matrix elements $|M_{x'}|^2$ have an elliptical distribution with the twofold symmetry axis in these QW planes. From a mathematical perspective, $(b^2+c^2+d^2+e^2)$ and f^2 terms in the in-plane matrix element, $|M_{x'}|^2$, are independent of the in-plane angle, α, and hence, the strength variation of the in-plane matrix element is proportional to the term "*d*". Meanwhile, a factor $(\cos\alpha \sin\alpha)$ appears in the term *d*, and therefore the optical twofold axis is not coincident with the $\alpha=0$ principal axis of the QW plane. However, this factor disappears in the $\{11\ell\}$ family since $\sin 4\gamma=0$. Hence, the tilted twofold optical axis occurs in the (123) QW plane, but not exists in the (110) or (113) planes, as can be seen in Figs. 5(a)–5(c). Since the (001) and (111) QWs belong to high symmetry point groups, their optical matrix elements have an isotropic curve in the QW plane, whose layer-plane curves are deliberately not shown in the figures in order to maintain clarity.

Generally, the in-plane optical anisotropy, ρ, of $(hk\ell)$-oriented QWs is defined as

$$\rho = \frac{|M_{x'}|^2 - |M_{y'}|^2}{|M_{x'}|^2 + |M_{y'}|^2}, \tag{20}$$

where $|M_{x'}|^2$ and $|M_{y'}|^2$ are the squared momentum matrix elements for the polarization parallel to the in-plane x' direction and y' direction, respectively. Furthermore, the in-plane optical anisotropy, ρ, can be written as

$$\rho = \frac{-2\sqrt{3}\, df}{b^2 + c^2 + d^2 + e^2 + 3f^2} \tag{21}$$

for the $(hk\ell)$ QWs.

By setting $\gamma=45°$, the anisotropy, ρ, of the (11ℓ) QWs can be expressed as

$$\rho = \frac{2\sqrt{3}(\cos^2\alpha - \sin^2\alpha)\sin\beta\left(1-\frac{3}{2}\sin^2\beta\right)(G' \pm \Delta')}{(4-3\sin^2\beta)\left(1-\frac{3}{2}\sin^2\beta\right)^2 + 3(G' \pm \Delta')^2}, \tag{22}$$

where

$$\Delta' = \sqrt{G'^2 + (4-3\sin^2\beta)(1-3\sin^2\beta/2)^2} \tag{23a}$$

and

$$G' = \frac{(E_{xx} - E_{zz} - 2E_{xy})\sin^2\beta\left(2-\frac{3}{2}\sin^2\beta\right) - \frac{2}{3}(E_{xx} - E_{zz})}{(E_{xx} - E_{zz} - 2E_{xy})\frac{1}{\sqrt{3}}\sin\beta}. \tag{23b}$$

To identify the maximum ρ value for each QW plane, theoretical calculations are performed for all of the in-plane angles ($\alpha: 0° \sim 360°$). Figures 6(a) and 6(b) illustrate the maximum ρ values of the *c-hh* and *c-lh* transitions for each $(hk\ell)$ QW plane, respectively, as a function of the substrate orientation in the first octant. Meanwhile, Fig. 7 indicates the ρ peak values of the *c-hh* and *c-lh* transitions for each (11) QW plane. The ρ value reaches its peak value on the (110) QW plane and its equivalent planes for both the *c-hh* and *c-lh* transitions. Moreover, the calculation results reveal that no in-plane anisotropy of the

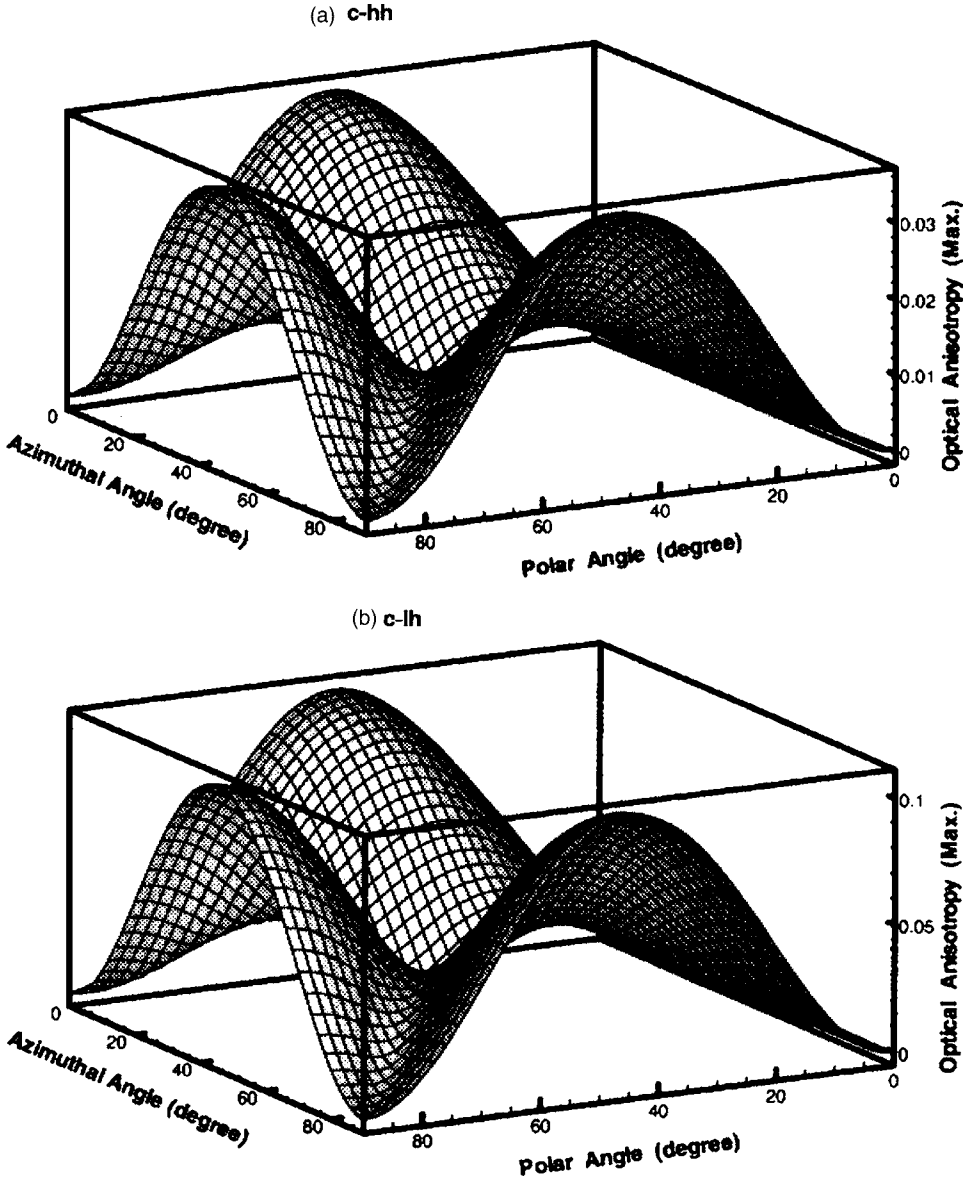

FIG. 6. In-plane optical anisotropy maximum of the (a) *c-hh* and (b) *c-lh* transitions for each $(hk\ell)$ $In_{0.53}Ga_{0.47}As$ QW plane as a function of the substrate orientation in the first octant. Note that the anisotropy maximum for each well plane is identified by considering all of the in-plane polarization angles ($\alpha=0°$–$360°$).

optical matrix elements is induced for structures grown on (001) or (111) substrates. As can be readily observed from Eq. (22), the in-plane optical anisotropy, ρ, is equal to zero for the (001) and (111) planes, corresponding to angles β of 0 and $\sin^{-1}\sqrt{2}/\sqrt{3}$, respectively. Other than the (001) and (111) planes, the anisotropy, ρ, belongs to an in-plane twofold symmetry, owing to the fact that the ρ value is in period of the in-plane angle by 180°. The anisotropy, ρ, is a result of the microscopic symmetry of the QW lattice. Since the (001) and (111)-oriented QWs belong to the D_{4h} and D_{3d} high-symmetry point groups, respectively, their polarization properties of the optical matrix elements are isotropic in the layer plane. Furthermore, other QW orientations have only low twofold symmetry, e.g., D_{2h} for (110), and hence, their polarization properties are presented in anisotropy on the QW planes. A fundamental consequence of symmetry reduction is that the interplay of the zone-center mixing leads to anisotropy. Generally speaking, the degree of anisotropy is affected by the geometrical arrangement of the lattice struc-

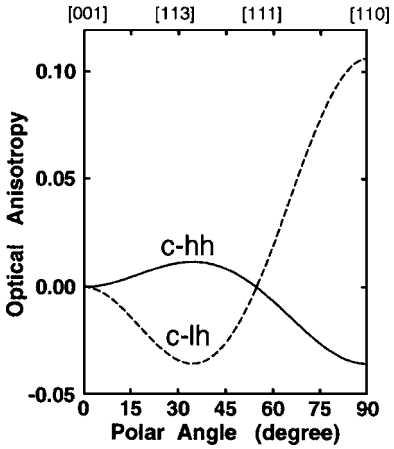

FIG. 7. In-plane optical anisotropy of the *c-hh* and *c-lh* transitions for each (11ℓ) $In_{0.53}Ga_{0.47}As$ QW plane as a function of the substrate orientation in the first octant.

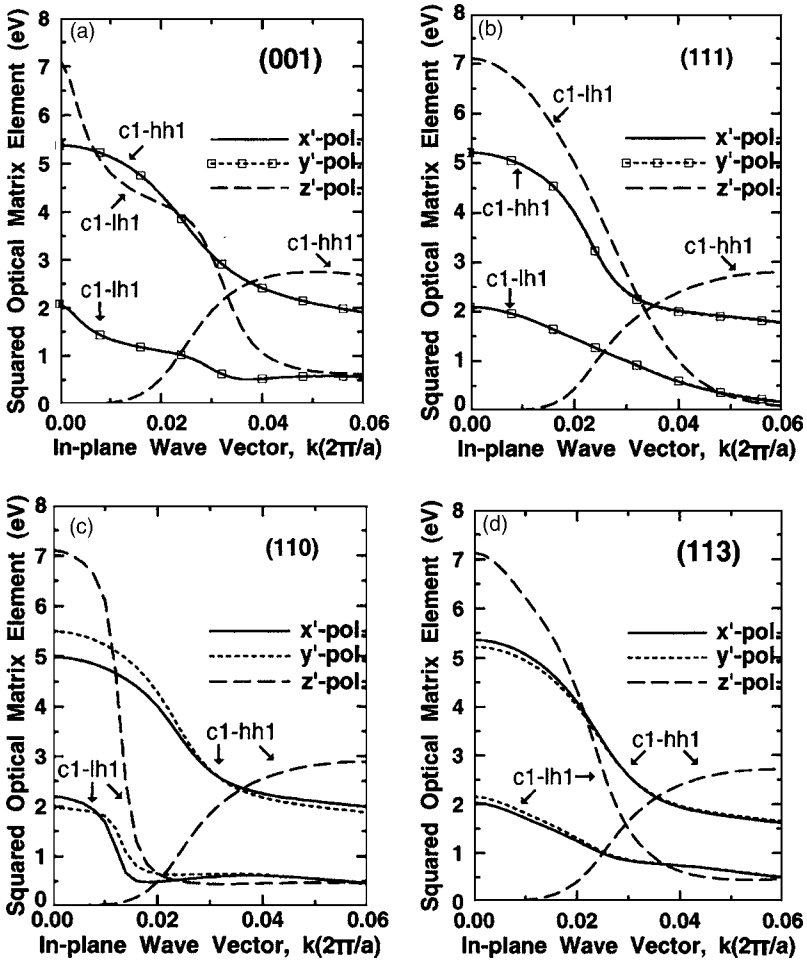

FIG. 8. Squared optical matrix elements (in units of electron-volts) of the $c1$-$hh1$ and $c1$-$lh1$ transitions for (a) (001), (b) (111), (c) (110), and (d) (113) $In_{0.53}Ga_{0.47}As/InP$ QWs as a function of the in-plane wave vector.

ture, which is a necessary consequence of the lower symmetry.

Without the approximations adopted in this section,[3,5,28] the momentum matrix elements, and thus the optical anisotropy ρ, are dependent on the well width of the QWs, even for an infinite-barrier-height case. The optical anisotropy is, in general, expected to increase with decreasing the well width for narrow wells, but not obviously for wide wells, as calculated for (110) QWs using the six-band Luttinger–Kohn Hamiltonian by Kajikawa.[29] Note that the conservation and sum rules are satisfied for the entire well-width range in the infinite-barrier-height case.

C. Momentum matrix elements under finite-barrier-height reality

In reality, the barrier height of the QWs is finite. Adopting this finite-barrier-height reality, Figs. 8(a)–8(d) present the squared optical matrix elements for the 60 Å width (001), (111), (110), and (113)-oriented $In_{0.53}Ga_{0.47}As/InP$ QWs without strain effects included, respectively. In these figures, $c1$, $hh1$, and $lh1$ denote the first subband of the conduction, heavy-hole, and light-hole bands, respectively. Furthermore, the band offsets of the conduction and valence bands in these $In_{0.53}Ga_{0.47}As/InP$ QWs are 143 and 346 meV, respectively. At low values of the in-plane wave vector, the in-plane band-mixing effect is small, and hence, almost pure states exist. Consequently, the band edge transition strengths of Figs. 8(a)–8(d) agree well with the predictions for the relative transition strength suggested by Figs. 1(a) and 1(b): Transitions from $c1$-$hh1$ favor TE modes, while transitions from $c1$-$lh1$ favor TM modes. TE and TM denote the light polarized parallel and perpendicular to the well plane, respectively. The $c1$-$hh1$ transition strength is large for TE modes, but vanishes for TM modes near the zone center. In contrast to other band edge transitions, the $c1$-$lh1$ transition strength of the TM modes reaches a maximum relative to any polarization light. Away from the zone center, the situation becomes more complicated due to the band mixing effects at finite in-plane wave vector. In contrast to Figs. 1(a) and 1(b), the total transition strength of the three orthogonal polarization directions is no longer conserved in a given subband transition, but decreases as the in-plane wave vector increases. The mixing effect between the various subbands results in a redistribution of the total transition strength among the various subband transitions.[25] Therefore, the $c1$-$hh1$ band edge transition of the TM mode is forbidden, but it picks up some finite transition strength away from the band edge. Owing to the redistribution of the total transition strength among the various subband transitions, some forbidden transitions can be observed.

Zone center mixing exists particularly in the low symmetry (110) and (113) QWs. Therefore, the in-plane anisotropy observed in Fig. 7 is also evident near the zone center in

Figs. 8(a)–8(d). For both the $c1$-$hh1$ and $c1$-$lh1$ transitions, the largest in-plane polarization of the optical matrix elements is located on the (110) QW plane, while the subsidiary polarization is found on the (113) QW plane. However, the in-plane polarization of the optical matrix elements is not found on the (001) and (111) QW planes due to the high symmetry of these particular planes. This observation is consistent with previous experimental results.[3,8,10] The present calculations reveal the obvious occurrence of zone-center mixing, which yields significant anisotropy effects.

D. Other factors in optical anisotropy

The local symmetry effect at the atomic scale is generally neglected in the $\mathbf{k}\cdot\mathbf{p}$ calculations due to the unit-cell-scale basis.[16–19] In zinc-blende semiconductors, $\mathbf{k}\cdot\mathbf{p}$ terms of tetragonal symmetry (odd-in-k terms) exist.[30–32] These terms correspond to the reduction of symmetry from O_h to T_d. The inversion asymmetry of the tetragonal bonds in zinc-blende semiconductors is shown to result in the anisotropy of the band structure in the vicinity of the Γ point and, consequently, in the anisotropy of the optical properties near the zone center.[33,34] The ionic tetragonal bonds in zinc-blende semiconductors play an important role in defining the near band-edge optical properties. When optical and/or external electrical fields interact with the permanent dipole moment of zinc-blende bonds, the interaction brings the inherent asymmetry of the tetragonal bonding states into the Hamiltonian. Thus field-induced optical anisotropy exists in zinc-blende structures.[33,34]

The epitaxial layer is commonly strained as a result of misfit with the substrate. The lattice-mismatch-generated strain reduces the symmetry of the zinc-blende crystal from cubic to tetragonal.[30,35] Furthermore, the strain breaks the crystal symmetry, which leads to tetragonally distorted unit-cells, zone-center mixing among the different band states, and built-in piezoelectric fields. As a consequence, strain-induced effects can produce additional optical anisotropy in zinc-blende semiconductor systems.[1,36]

When considering valence band warping (i.e., the anisotropy of in-plane effective mass of holes), the $(hk\ell)$ QWs exhibit additional in-plane anisotropy of the optical properties, even for the (001) and (111) QWs. The reason for this is that the probabilities of the interband transitions depend on the reduced density of states, which is expressed as the effective mass of the interaction carriers. These phenomena have been observed in hot-photoluminescence experiments and have also been investigated theoretically.[30,37,38] For electrons excited from the valence to the conduction bands with linearly polarized laser light, the anisotropically angular distribution in number, momentum, and energy of the photoexcited hot electrons reflects the warping of the valence band. As a consequence, this distribution determines the in-plane optical anisotropy of the luminescence arising from the recombination of hot electrons with neutral acceptor states.[30,39,40] Furthermore, this valence band warping yields an energy spread of the resulting luminescence at neutral acceptors by hot electrons excited by the different polarized-direction lights. Valence band warping also depends on the frequency of the resulting luminescence.[41]

IV. CONCLUSIONS

This study has presented the derivation of general expressions for the analytical $\mathbf{k}\cdot\mathbf{p}$ Hamiltonian which are valid for arbitrary substrate orientations. Using the analytical $\mathbf{k}\cdot\mathbf{p}$ method, this study has also developed explicit mathematical expressions for the optical transition strength, which enable the linearly polarized anisotropy to be explored. The origin of optical anisotropy in quantum wells has been investigated, and it has been proven theoretically that this phenomenon can be attributed to low-symmetry perturbations of the zinc-blende lattice. As expected from qualitative symmetry arguments, the theoretical findings reported in this study are in good agreement with the experimental results of previous studies. It has been shown that the (110) quantum well plane exhibits the largest anisotropy of any substrate plane, while the (001) and (111) quantum well planes are completely polarization independent for the optical matrix elements. Furthermore, the efficient methods presented in this study are beneficial to the design of optical devices fabricated on any substrate orientation. One of the main applications of the present method could also be for the analysis of the polarization properties of hot photoluminescence in quantum well structures. Finally, the current investigation provides valuable guidelines for the design of polarization stabilization devices, which require polarization control or selectivity.

ACKNOWLEDGMENT

This study was partially supported by the National Science Council of the Republic of China, Taiwan.

APPENDIX A

The matrix elements of the 6×6 $\mathbf{k}\cdot\mathbf{p}$ Hamiltonian $H_{\mathbf{k}\cdot\mathbf{p}}(\mathbf{k})_{\nu',\nu}$ [in the basis ordering (ν=1–6) corresponding to $|S\rangle\chi_{\sigma=1/2}, |S\rangle\chi_{\sigma=-1/2}, |3/2,3/2\rangle, |3/2,1/2\rangle, |3/2,-1/2\rangle, |3/2,-3/2\rangle$, respectively] are given by

$$H_{11}=H_{22}=(E_s+12E_{ss})-E_{ss}a^2\mathbf{k}^2,$$

$$\begin{aligned}H_{33}&=H_{66}\\&=(E_p+8E_{xx}+4E_{zz})-[(3E_{xx}+E_{zz})/4]a^2\mathbf{k}^2\\&\quad+[(E_{xx}-E_{zz})/4]a^2k_z^2,\end{aligned}$$

$$\begin{aligned}H_{44}=H_{55}&=(E_p+8E_{xx}+4E_{zz})-[(7E_{xx}+5E_{zz})/12]a^2\mathbf{k}^2\\&\quad-[(E_{xx}-E_{zz})/4]a^2k_z^2,\end{aligned}$$

$$H_{13}=\sqrt{3}H_{15}^*=\sqrt{3}H_{24}=H_{26}^*=-i2\sqrt{2}E_{sx}a(k_x+ik_y),$$

$$H_{14}=H_{25}=i8aE_{sx}k_z/\sqrt{6},$$

$$H_{34}=-H_{56}=\frac{a^2}{\sqrt{3}}E_{xy}(k_x-ik_y)k_z,$$

and

$$H_{35} = H_{46} = \frac{a^2}{4\sqrt{3}}[(E_{xx} - E_{zz})(k_x^2 - k_y^2) - i4E_{xy}k_xk_y],$$

where the superscript *denotes the Hermitian conjugate. Note that the $\mathbf{k}\cdot\mathbf{p}$ Hamiltonian is Hermitian, which results in $H_{ij}=H_{ji}^*$ with $i,j=1$–6. Other than the matrix elements depicted above, all other elements are equal to zero.

APPENDIX B

(1) *x*-polarization matrix elements in finite difference scheme.

The *x*-polarization matrix $\boldsymbol{\varepsilon}_x\cdot\mathbf{O}_{\nu',\nu}(\mathbf{k}_\parallel,z)$ in the same basis ordering as the Hamiltonian is written as

$$O_{11} = O_{22} = -2a^2E_{ss}k_x,$$

$$O_{33} = O_{66} = -[(3E_{xx} + E_{zz})/2]a^2k_x,$$

$$O_{44} = O_{55} = -[(7E_{xx} + 5E_{zz})/6]a^2k_x,$$

$$O_{13} = \sqrt{3}O_{15}^* = \sqrt{3}O_{24} = O_{26}^* = -i2\sqrt{2}aE_{sx},$$

$$O_{35} = O_{46} = \frac{a^2}{2\sqrt{3}}[(E_{xx} - E_{zz})k_x - i2E_{xy}k_y],$$

$$O_{ij} = O_{ji}^* \quad \text{with} \quad i,j = 1\text{–}6,$$

and the remaining matrix elements are equal to zero.

The *x*-polarization matrix $\boldsymbol{\varepsilon}_x\cdot\mathbf{Q}_{\nu',\nu}(\mathbf{k}_\parallel,z)$ in the same basis ordering as the Hamiltonian is written as

$$Q_{34} = Q_{43}^* = -Q_{56} = -Q_{65}^* = \frac{a^2}{\sqrt{3}}E_{xy},$$

and the remaining matrix elements are equal to zero.

(2) *y*-polarization matrix elements in finite difference scheme.

The *y*-polarization matrix $\boldsymbol{\varepsilon}_y\cdot\mathbf{O}_{\nu',\nu}(\mathbf{k}_\parallel,z)$ in the same basis ordering as the Hamiltonian is written as

$$O_{11} = O_{22} = -2a^2E_{ss}k_y,$$

$$O_{33} = O_{66} = -[(3E_{xx} + E_{zz})/2]a^2k_y,$$

$$O_{44} = O_{55} = -[(7E_{xx} + 5E_{zz})/6]a^2k_y,$$

$$O_{13} = \sqrt{3}O_{15}^* = \sqrt{3}O_{24} = O_{26}^* = 2\sqrt{2}aE_{sx},$$

$$O_{35} = O_{46} = -\frac{a^2}{2\sqrt{3}}[(E_{xx} - E_{zz})k_y + i2E_{xy}k_x],$$

$$O_{ij} = O_{ji}^* \quad \text{with} \quad i,j = 1 \sim 6,$$

and the remaining matrix elements are equal to zero.

The *y*-polarization matrix $\boldsymbol{\varepsilon}_y\cdot\mathbf{Q}_{\nu',\nu}(\mathbf{k}_\parallel,z)$ in the same basis ordering as the Hamiltonian is written as

$$Q_{34} = Q_{43}^* = -Q_{56} = -Q_{65}^* = -i\frac{a^2}{\sqrt{3}}E_{xy},$$

and the remaining matrix elements are equal to zero.

(3) *z*-polarization matrix elements in finite difference scheme

The *z*-polarization matrix $\boldsymbol{\varepsilon}_z\cdot\mathbf{O}_{\nu',\nu}(\mathbf{k}_\parallel,z)$ in the same basis ordering as the Hamiltonian is written as

$$O_{14} = O_{25} = i\frac{8}{\sqrt{6}}aE_{sx},$$

$$O_{34} = -O_{56} = \frac{a^2}{\sqrt{3}}E_{xy}(k_x - ik_y),$$

$$O_{ij} = O_{ji}^* \quad \text{with} \quad i,j = 1 \sim 6,$$

and the remaining matrix elements are equal to zero.

The *z*-polarization matrix $\boldsymbol{\varepsilon}_z\cdot\mathbf{Q}_{\nu',\nu}(\mathbf{k}_\parallel,z)$ in the same basis ordering as the Hamiltonian is written as

$$Q_{11} = Q_{22} = -2a^2E_{ss},$$

$$Q_{33} = Q_{66} = -(E_{xx} + E_{zz})a^2,$$

$$Q_{44} = Q_{55} = -[(5E_{xx} + E_{zz})/3]a^2,$$

and the remaining matrix elements are equal to zero.

*Electronic address: chen3018@ms76.hinet.net

[1] R. H. Henderson and E. Towe, J. Appl. Phys. **79**, 2029 (1996).
[2] Y. Kajikawa, M. Hata, N. Sugiyama, and Y. Katayama, Phys. Rev. B **42**, 9540 (1990).
[3] Y. Kajikawa, O. Brandt, K. Kanamoto, and N. Tsukada, J. Cryst. Growth **150**, 431 (1995).
[4] Y. Kajikawa, J. Appl. Phys. **86**, 5663 (1999).
[5] Y. Kajikawa, Phys. Rev. B **47**, 3649 (1993).
[6] R. H. Henderson and E. Towe, J. Appl. Phys. **78**, 2447 (1995).
[7] C. N. Chen, J. Appl. Phys. **96**, 7374 (2004).
[8] Y. Kajikawa, M. Hata, T. Isu, and Y. Katayama, Surf. Sci. **267**, 501 (1992).
[9] D. S. McCallum, X. R. Huang, and A. L. Smirl, Appl. Phys. Lett. **66**, 2885 (1995).
[10] G. Armelles, P. Castrillo, P. S. Dominguez, L. Gonzalez, A. Ruiz, D. A. Contreras-Solorio, V. R. Velasco, and F. Garcia-Moliner, Phys. Rev. B **49**, 14020 (1994).
[11] R. H. Henderson, D. Sun, and E. Towe, Surf. Sci. **327**, L521 (1995).
[12] G. Shechter, L. D. Shvartsman, and J. E. Golub, Phys. Rev. B **51**, 10857 (1995).
[13] R. A. Abram and M. Jaros, *Band Structure Engineering in Semi-*

conductor Microstructures (Plenum, New York, 1989).
[14] A. Niwa, T. Ohtoshi, and T. Kuroda, IEEE J. Sel. Top. Quantum Electron. **1**, 211 (1995).
[15] J. B. Xia, Phys. Rev. B **43**, 9856 (1991).
[16] E. O. Kane, in *Semiconductors and Semimetals*, edited by R. K. Willardson and A. C. Beer (Academic, New York, 1966), Vol. 1, p. 75.
[17] J. M. Luttinger, Phys. Rev. **102**, 1030 (1956).
[18] Y. C. Chang, Phys. Rev. B **37**, 8215 (1988).
[19] S. F. Tsay, J. C. Chiang, Z. M. Chau, and I. Lo, Phys. Rev. B **56**, 13242 (1997).
[20] C. N. Chen, Y. H. Wang, M. P. Houng, and J. C. Chiang, Jpn. J. Appl. Phys., Part 1 **41**, 36 (2002).
[21] Z. Ikonic, V. Milanovic, and D. Tjapkin, Phys. Rev. B **46**, 4285 (1992).
[22] F. Szmulowicz, Phys. Rev. B **51**, 1613 (1995).
[23] Y. C. Chang and R. B. James, Phys. Rev. B **39**, 12672 (1989).
[24] W. Ludwig and C. Falter, *Symmetries in Physics* (Springer-Verlag, Berlin, 1988), p. 30.
[25] P. S. Zory, *Quantum Well Lasers* (Academic, San Diego, 1993), p. 53.
[26] A. A. Yamaguchi, K. Nishi, and A. Usui, Jpn. J. Appl. Phys., Part 2 **33**, L912 (1994).
[27] N. A. Merkulov, V. I. Perel', and M. E. Portnoi, Sov. Phys. JETP **72**, 669 (1991).
[28] M. V. Belousov, E. L. Ivchenko, and A. I. Nesvizhskii, Phys. Solid State **37**, 763 (1995).
[29] Y. Kajikawa, Phys. Rev. B **51**, 16790 (1995).
[30] E. L. Ivchenko and G. E. Pikus, *Superlattices and Other Heterostructures: Symmetry and Optical Phenomena* (Springer-Verlag, Berlin, 1995).
[31] M. Cardona, N. E. Christensen, and G. Fasol, Phys. Rev. B **38**, 1806 (1988).
[32] F. G. Pikus and G. E. Pikus, Phys. Rev. B **51**, 16928 (1995).
[33] J. B. Khurgin and P. Voisin, Phys. Rev. Lett. **81**, 3777 (1998).
[34] J. B. Khurgin and P. Voisin, Semicond. Sci. Technol. **12**, 1378 (1997).
[35] G. L. Bir and G. E. Pikus, *Symmetry and Strain-induced Effects in Semiconductors* (Wiley, New York, 1974).
[36] Y. Kajikawa, Phys. Rev. B **49**, 8136 (1994).
[37] D. N. Mirlin and V. I. Perel', Semicond. Sci. Technol. **7**, 1221 (1992).
[38] D. S. Kainth, M. N. Khalid, and H. P. Hughes, Solid State Commun. **122**, 351 (2002).
[39] M. E. Portnoi, Sov. Phys. Semicond. **25**, 1294 (1991).
[40] P. S. Kop'ev, D. N. Mirlin, D. G. Polyakov, I. I. Reshina, V. F. Sapega, and A. A. Sirenko, Sov. Phys. Semicond. **24**, 757 (1990).
[41] J. A. Kash, M. Zachau, M. A. Tischler, and U. Ekenberg, Phys. Rev. Lett. **69**, 2260 (1992).